microorganisms

MDPI

Article

Investigating the Effect of Biofungicides on Grape Microbiomes in Central Coast of California

Kallol Das [1], Edgar Godoy Monterroso [1], Shijian Zhuang [2], Shashika S. Hewavitharana [1,3] and Shunping Ding [1,4,*]

[1] Plant Sciences Department, California Polytechnic State University, San Luis Obispo, CA 93407, USA; kdas01@calpoly.edu (K.D.); egodoymo@calpoly.edu (E.G.M.); shewavit@calpoly.edu (S.S.H.)
[2] University of California Cooperative Extension, Fresno, CA 93710, USA; gzhuang@ucanr.edu
[3] Strawberry Center, California Polytechnic State University, San Luis Obispo, CA 93407, USA
[4] Wine and Viticulture Department, California Polytechnic State University, San Luis Obispo, CA 93407, USA
* Correspondence: sding01@calpoly.edu

Abstract

Understanding how biofungicides affect grape-associated microbiomes is crucial for developing sustainable viticulture practices. In this study, eight distinct treatments, including synthetic fungicides, biofungicides *Bacillus subtilis*-based (Bs); *Streptomyces lydicus*-based (Sl); *Reynoutria sachalinensis* extract (Rs), and untreated controls, were evaluated to compare the bacterial and fungal communities that reside on the surfaces of 64 berry samples (32 samples per year) of *Vitis vinifera* cv. "Pinot Noir" grown in the Central Coast of California over two growing seasons (2023–2024). High-throughput 16S rRNA gene sequencing and ITS sequencing were used to explore the berry surface microbiome data for the bacterial and fungal assemblages. Beta-diversity analyses and heatmaps showed substantial replicate-to-replicate variation, particularly in fungal communities, without consistent treatment-specific clustering. In 2023, *Bacillus velezensis* (11.40%), *Methylobacterium adhaesivum* (17.05%), and *Staphylococcus pasteuri* (6.41%) were the most common bacteria on grape skins. In 2024, *Bacillus atrophaeus* (6.70%) and *Hydrotalea flava* (6.01%) became the most common bacteria, along with comparable contributions from genera *Bosea* and *Xanthomonas*. The fungal communities were made up of a few dominant species, such as *Cladosporium chasmanthicola* (16.49%), *C. puyae* (14.02%), *C. herbarum* (11.78%), *C. rhusicola* (7.15%), *C. angustiherbarum* (6.61%), *C. ipereniae* (4.33%), and *Aureobasidium leucospermi* (4.23%) in 2023; and *C. chasmanthicola* (38.01%), *C. puyae* (11.49%), *C. herbarum* (8.30%), *Aureobasidium pullulans* (6.20%), *Alternaria infectoria* (5.03%), and *Erysiphe necator* (4.24%) in 2024. PERMANOVA indicated significant treatment-associated differences in bacterial and fungal community composition in both years (bacteria: $R^2 = 0.308$–0.362, $p < 0.0001$; fungi: $R^2 = 0.312$–0.325, $p = 0.0011$–0.0106), with no evidence of heterogeneous multivariate dispersion among treatments (PERMDISP, $p = 0.1131$–0.8780). Although bacterial richness and Shannon diversity did not differ significantly among treatments, and fungal alpha diversity was generally similar among treatments except for a marginal effect on Shannon diversity observed in 2024, PERMANOVA indicated treatment-associated differences in the relative composition of both bacterial and fungal communities. Overall, fungicide programs were associated with shifts in grape berry-surface microbial composition; however, their effects on disease suppression and vineyard performance require validation using disease-incidence, yield, and fruit-quality data.

Check for updates

Academic Editor: Gary A. Strobel

Received: 29 August 2026
Revised: 5 November 2026
Accepted: 6 November 2026
Published: 18 November 2026

Copyright: © 2026 by the authors. Licensee MDPI, Basel, Switzerland. This article is an open access article distributed under the terms and conditions of the Creative Commons Attribution (CC BY) license.

Keywords: grape microbiome; Pinot Noir; biofungicides; bacterial and fungal communities; sustainable viticulture

1. Introduction

Grapevine (*Vitis vinifera* L.) is embedded in a rich phyllosphere and carposphere microbiome that evolves over the growing season and can influence vine health, disease outcomes, wine quality, and ultimately fruit integrity [1,2]. Culture-independent surveys showed that grape-associated communities are shaped by cultivar, soil properties including pH, moisture, texture, nutrient status, and salinity, as well as climatic conditions including temperature, rainfall, solar radiation, humidity, and wind [3,4]. For cultivars such as "Pinot Noir", whose fruit quality is tightly coupled to disease pressure and canopy microclimate, understanding the ecology of these surface communities is especially consequential [3,5]. In recent years, the concept of the "grapevine holobiont" has emerged, highlighting the importance of complex microbial consortia inhabiting different plant compartments, including the rhizosphere (root-associated soil), phyllosphere (above-ground plant surfaces), endosphere (internal plant tissues), and carposphere (fruit surface). This study focused exclusively on the carposphere, defined as the microbial community on grape berry surfaces; rhizosphere and endosphere communities were not evaluated. These microbial communities play crucial roles in nutrient cycling, resistance to abiotic stress, and suppression of phytopathogens [6,7]. The phyllosphere microbiome, in particular, directly influences the initial microbial composition of grapes and, consequently, the fermentation process that shapes wine characteristics [3]. Studies have shown that the structure of these communities is determined by cultivar, geography, vineyard management practices, and climatic conditions [8,9]. The grapevine phyllosphere represents a complex microbial habitat in which community composition and microbe–microbe interactions are associated with grapevine health, highlighting the importance of characterizing phyllosphere microbial communities under different vineyard conditions [1]. Microbial communities associated with grape berry surfaces may contribute to disease resistance and are influenced by vineyard-specific environmental factors [8]. Genera such as *Methylobacterium* contribute to plant growth promotion, whereas yeasts like fungi, such as *Aureobasidium* and *Cryptococcus*, are recognized for their biocontrol potential against pathogenic fungi [10–12]. Conversely, the relative abundances of fungal taxa, including *Cladosporium* spp. and *Erysiphe necator*, vary with cultivar, geographic region, vintage, and climatic conditions [3]. Recent vineyard studies highlighted the importance of balancing microbial richness and evenness, as high richness does not necessarily correlate with pathogen suppression if opportunistic pathogens are simultaneously enriched [10,13].

One of the major threats to grapevine cultivation is the prevalence of fungal diseases such as powdery mildew (caused by *E. necator*) and Botrytis bunch rot (caused by *Botrytis cinerea*), both of which thrive under favorable vineyard conditions and can devastate yield and quality [14–16]. Traditionally, disease management has relied heavily on synthetic fungicides, which provide effective control but are associated with multiple drawbacks. Continuous use of chemical inputs not only drives fungicide resistance among pathogen populations but may also disrupt beneficial microbial assemblages, reduce biodiversity, and contribute to environmental contamination [17,18]. Biofungicides derived from microbial antagonists represent a promising alternative to conventional fungicides. Formulations based on *Bacillus* spp. (e.g., Serenade), *Streptomyces* spp. (e.g., Actinovate), and botanical extracts of *Reynoutria sachalinensis* (Regalia) have gained increasing popularity in viticulture for their dual capacity to suppress pathogens and promote beneficial microbial communities [19–21]. Their modes of action include antibiosis, competition for nutrients and

niches, induction of host plant resistance, and modulation of microbial networks in the phyllosphere [22]. However, little is known about how *R. sachalinensis* extract, applied alone or rotated with synthetic fungicides, influences bacterial and fungal communities on grape berry surfaces. For instance, *Bacillus velezensis* and *B. atrophaeus* are well-documented producers of lipopeptides such as surfactin and iturin, which disrupt fungal pathogens while simultaneously encouraging microbial community stability [23]. However, few field-based studies have directly compared specific biofungicide products and application frequencies to determine their impact on both bacterial and fungal community structures across multiple growing seasons. Such a study stands to refine IPM in cool-coastal winegrape cultivar "Pinot Noir" and to advance a microbiome-aware viticulture that balances disease control with stewardship of the living canopy [3,24].

Biofungicides become increasingly integrated into commercial viticulture; thus, it is essential to elucidate the role of vineyard microbiomes in grapevine health and wine quality, and to assess how these treatments alter microbial community composition. The present study was designed to provide a comparative analysis of microbial communities associated with "Pinot Noir" grape surfaces in the Central Coast of California. Specifically, we investigated how applications of Bs (*Bacillus subtilis*), Sl (*Streptomyces lydicus*), Rs (*Reynoutria sachalinensis*), their combinations with synthetics, and synthetic-only treatments affect bacterial and fungal carposphere communities. The findings are intended to support the development of sustainable management practices that balance disease suppression with the preservation of beneficial microbial networks in vineyards. Ultimately, this research contributes to the broader field of plant–microbiome interactions, highlighting how targeted manipulation of microbial assemblages can strengthen the resilience of cropping systems in environmental and pathogen pressures.

2. Materials and Methods

2.1. Site Description

The investigation was carried out in a vineyard in San Luis Obispo, California (35.32026° N, 120.68404° W). The cultivar "Pinot Noir", which was planted in 2017, was selected for this study. The vineyard was managed under commercial standards, such as suckering, shoot thinning, wire lifting, leaf pulling, and weeding.

2.2. Experimental Design

Treatments were arranged in a randomized complete block design (RCBD) with four blocks (replicates) in the vineyard, and each treatment appeared once per block. Three biofungicides were evaluated in this study: Regalia (Rs; 5% extract of *Reynoutria sachalinensis*), Actinovate (Sl; 0.037% *Streptomyces lydicus* strain WYEC 108), and Serenade (Bs; 1.34% *Bacillus subtilis* strain QST 713). The experiment included 8 treatments, and the treatments consisted of: Rs applied weekly; Rs rotated with synthetic fungicides; Sl applied weekly; Sl rotated with synthetic fungicides; Bs applied weekly; Bs rotated with synthetic fungicides; the grower standard consisting of synthetic fungicides applied biweekly; and an untreated control (UTC). Eight treatments were arranged in four blocks, yielding 32 experimental plots in total. Treatment codes A–H used in the sample IDs, heatmaps, and supplementary dataset corresponded to the treatment names listed above; numbers R1–R4 indicated replicate plots (Table 1). The weekly biofungicide programs received 12 applications in both 2023 and 2024. Rotational programs alternated the respective biofungicide with synthetic fungicides, and the grower-standard program received synthetic fungicides only. Detailed fungicide application schedules, commercial products, active ingredients, rates, and numbers of applications for each treatment program in 2023 and 2024 are provided in

Supplementary File S1. Because product identity and application schedules differed among treatment programs, their individual effects cannot be separated.

Table 1. Treatment codes, fungicide programs, and corresponding sample identifiers for the four biological replicates used in this study.

Treatment Code	Treatment	Sample IDs & Replications
A (01)	*Reynoutria sachalinensis* (Rs) applied on weekly basis	A.V01.R1, A.W01.R2, A.X01.R3, A.Y01.R4
B (04)	Rs integrated in a synthetic fungicide program	B.V04.R1, B.W04.R2, B.X04.R3, B.Y04.R4
C (05)	*Streptomyces lydicus* (Sl) applied on weekly basis	C.V05.R1, C.W05.R2, C.X05.R3, C.Y05.R4
D (08)	Sl integrated in a synthetic fungicide program	D.V08.R1, D.W08.R2, D.X08.R3, D.Y08.R4
E (09)	*Bacillus subtilis* (Bs) applied on weekly basis	E.V09.R1, E.W09.R2, E.X09.R3, E.Y09.R4
F (12)	Bs integrated in a synthetic fungicide program	F.V12.R1, F.W12.R2, F.X12.R3, F.Y12.R4
G (13)	All synthetics	G.V13.R1, G.W13.R2, G.X13.R3, G.Y13.R4
H (14)	Untreated control (UTC)	H.V14.R1, H.W14.R2, H.X14.R3, H.Y14.R4

Note: Regalia formulation containing an extract of *Reynoutria sachalinensis*; Actinovate product based on *Streptomyces lydicus*; Serenade product based on *Bacillus subtilis*; and UTC, untreated control.

2.3. Sample Collection and Pre-Processing

Four grape clusters were collected approximately one week prior to commercial maturity from each plot, and this sampling strategy accounted for variation within each plot. From these clusters, five berries were randomly selected and pooled to form one composite sample per plot. Each composite sample was prepared using clusters collected from at least three grapevines. The harvested clusters were placed in sterile plastic bags and transported to the laboratory, kept at 4 °C until they were processed for further analysis. Samples were stored until the final product was obtained.

2.4. Sample Processing and DNA Extraction

The berry surfaces were aseptically peeled with sterile forceps and placed into 1.5 mL microcentrifuge tubes to recover microbial biomass for DNA extraction. Because surface-associated microorganisms can adhere strongly to the grape berry skin and cuticle [25], a modified methylene chloride–Tris buffer treatment was used to disrupt and remove the hydrophobic cuticular wax layer before microbial DNA extraction. Methylene chloride has been used to extract cuticular waxes from grape berry skins [26]. Peeled skins were immersed in 500 µL of Solution A (1:1 of methylene chloride and 1× Tris buffer with pH 8.0), mixed thoroughly, incubated for 2–4 h at room temperature, vortexed, to separate microbes from the skin; then the organic (methylene chloride) layer was removed and discarded. Then, an additional 200 µL of Solution A was added, and the samples were vortexed for 30 s to promote further detachment and separation of microorganisms remaining on the berry skins. The tubes were then centrifuged at 8000 rpm for 8 min to pellet the recovered microbial biomass. The supernatant was discarded, and pellets were left in a fume hood for ~3–4 h or longer to evaporate residual methylene chloride completely. After complete evaporation of residual methylene chloride, the dried pellet was stored at 4 °C until genomic DNA extraction.

2.5. DNA Extraction, PCR Amplification, and High-Throughput Sequencing

Total genomic DNA was extracted from berry surface samples using the DNeasy Plant Pro Kit (Qiagen, Hilden, Germany) according to the manufacturer's protocol. Bacterial communities were amplified using 16S rRNA for V5–V7 regions with the primers 799F (5′-AAC MGG ATT AGA TAC CCK G-3′) and 1193R (5′-ACG TCA TCC CCA CCT TCC-3′) [27],

and fungal communities using ITS regions with the primers ITS1F (5′-CTT GGT CAT TTA GAG GAA GTAA-3′) and ITS4 (5′-GCT GCG TTC TTC ATC GATGC-3′) [28,29]. Each 20 µL PCR contained 2 µL template DNA, 1 µL of each primer, 10 µL PCR Master Mix (Applied Biosystems, Warrington, UK), and 6 µL nuclease-free water. Thermal cycling for 16S was: 94 °C for 3 min; 35 cycles of 94 °C for 20 s, 53 °C for 40 s, 72 °C for 40 s; final extension at 72 °C for 7 min [27]. Cycling for ITS was: 94 °C for 5 min; 35 cycles of 94 °C for 45 s, 55 °C for 45 s, 72 °C for 45 s; final extension 72 °C for 10 min [28,29]. PCR amplification was performed as a single technical reaction for each biological sample. A no-template PCR control containing all reaction components except template DNA was included in each amplification batch. No visible amplification was detected in the negative controls; therefore, no contaminant zOTUs were identified. Amplicon-library preparation, sample barcoding, pooling, and Illumina MiSeq sequencing were performed by MR DNA (MR DNA, Shallowater, TX, USA) according to its standard amplicon-sequencing workflow. The 16S rRNA gene libraries from both 2023 and 2024 were sequenced on an Illumina MiSeq platform using paired-end approximately 2 × 250 bp reads. ITS libraries from 2023 were sequenced using paired-end 2 × 300 bp reads, whereas ITS libraries from 2024 were sequenced using 2 × 250 bp reads.

2.6. Bioinformatics, Metabarcoding and Statistical Analysis

Paired-end 16S rRNA gene and ITS amplicon reads were processed using the MR DNA ribosomal and functional-gene analysis pipeline (http://www.mrdnalab.com, accessed on 1 August 2026; MR DNA, Shallowater, TX, USA). Paired reads were joined, primer sequences were removed, and reads shorter than 150 bp, containing ambiguous bases, or exceeding a maximum expected-error threshold of 1.0 were excluded. Quality-filtered reads were dereplicated and denoised to remove sequencing and PCR errors, followed by chimera removal, generating zero-radius operational taxonomic units (zOTUs). Following denoising and chimera removal, no additional minimum-abundance or prevalence threshold was applied; all retained zOTUs were included in downstream analyses. Therefore, conventional 97% sequence-similarity OTU clustering was not performed. Representative zOTU sequences were taxonomically assigned using BLASTn against an MR DNA-curated (MR DNA version 2024.4), NCBI-derived reference database, and reads were mapped to generate zOTU count tables. Species-level assignments are reported as putative BLASTn-based annotations (www.ncbi.nlm.nih.gov; accessed on 13 February 2024). Non-fungal ITS assignments were excluded before fungal-community analyses. Species-level labels are reported as putative BLASTn-based annotations and should not be interpreted as definitive species identifications. According to the MR DNA identity-classification criteria, sequences with >97% identity to a reference sequence were designated at the species level; sequences with 95–97% identity were reported as unclassified at the genus level, with lower identity values assigned only to progressively higher taxonomic ranks. The Q25 sequence data derived from the sequencing process were processed using a standard analysis pipeline developed in-house by MR DNA (http://www.mrdnalab.com; Shallowater, TX, USA). For fungal-community analyses, only zOTUs included in the MR DNA "fungi" output were retained. Non-fungal eukaryotic assignments, including Metazoa and Viridiplantae, were excluded before calculation of relative abundance and all downstream analyses. For bacterial-community analyses, chloroplast- and mitochondrial-derived zOTUs were removed before calculation of relative abundance and all downstream analyses. No rarefaction was performed. All 32 samples were retained in each dataset. For each sample, final zOTU counts were converted to relative abundance. Relative-abundance-transformed zOTU data were used for heatmaps and beta-diversity analyses, including Bray–Curtis dissimilarities, PCoA, UPGMA clustering, PERMANOVA, and PERMDISP. Rarefaction curves were generated from final zOTU count matrices to assess sequencing coverage. Counts were

normalized within each sample and expressed as relative abundance (%). Taxonomic names were standardized throughout the datasets, figures, tables, and Supplementary File using traditional classifications where necessary to avoid ambiguity caused by nomenclatural changes [30].

Pairwise sample dissimilarities for the bacterial and fungal heatmaps were calculated using the Yue–Clayton thetaYC metric and visualized in Explicet software (v2.10.5) [31,32]. ThetaYC was used exclusively to visualize pairwise differences in zOTU community composition among individual samples. Bray–Curtis dissimilarities were used for PCoA and UPGMA hierarchical clustering; UPGMA clustering was performed using PAST (PAleontological STatistics) software (version 4.03) [33]. Permutational multivariate analysis of variance (PERMANOVA) was conducted separately for bacterial and fungal communities within each year using Bray–Curtis dissimilarities calculated from relative-abundance-transformed zOTU counts. The effects of fungicide treatments on Bray–Curtis community dissimilarities were tested after accounting for differences among the four experimental blocks. Analyses were performed in R version 4.3.2 (R Foundation for Statistical Computing, Vienna, Austria; https://www.R-project.org/, accessed on 1 August 2026) [34] using the vegan package version 2.6.10 [35], with 9999 permutations restricted within blocks. Homogeneity of multivariate dispersion was assessed using PERMDISP based on the same distance matrices and permutation scheme. Pairwise PERMANOVA tests were not conducted. Alpha diversity was calculated from the final unrarefied zOTU count matrices using Chao1 richness and Shannon diversity indices. Treatment effects were assessed separately for each year's dataset using a randomized complete block design, with treatment as a fixed factor and block (V, W, X, and Y) included as a blocking factor. Significance was assessed using restricted permutation tests (9999 permutations) in R. Statistical significance was set at $p < 0.05$. Relative-abundance summaries and visualizations were created in R [34].

3. Results

3.1. Sequencing Statistics

Sequencing depth differed substantially among datasets. Based on NCBI SRA RunInfo metadata, the mean number of raw paired-end read pairs per sample was 884,626 (range, 593,489–1,110,571) for 16S libraries in 2023, 289,878 (222,557–340,221) for 16S libraries in 2024, 98,798 (46,257–204,839) for ITS libraries in 2023, and 147,233 (55,245–271,139) for ITS libraries in 2024 (Supplementary File S2). After sequence processing, the 2023 bacterial dataset contained 12,836 retained reads across 32 samples, with 24–4776 reads per sample (mean, 401; median, 124 reads/sample). The 2024 bacterial dataset contained 132,216 retained reads, with 769–20,721 reads per sample (mean, 4132; median, 1842 reads/sample). Fungal datasets yielded 2,910,097 reads in 2023 (42,163–188,763 reads/sample; mean, 90,941; median, 82,051) and 1,112,432 reads in 2024 (33,490–34,938 reads/sample; mean, 34,764; median, 34,850). Rarefaction curves indicated variable sequencing coverage among datasets (Figure S1). The 2023 bacterial dataset had low and highly uneven sequencing depth (24–4776 reads/sample). Because rarefaction with the minimum library size of 24 reads per sample would be uninformative, bacterial results were interpreted separately within each year, and no between-year bacterial comparisons were performed. Several fungal rarefaction curves in 2024 increased, indicating that fungal taxon-level patterns and richness estimates should also be interpreted cautiously. Therefore, no formal between-year comparisons were performed for fungal communities, either.

3.2. Zero-Radius Operational Taxonomic Unit (zOTU) Analysis

Pairwise dissimilarity among individual biological replicate samples was visualized using Yue–Clayton thetaYC heatmaps (Figures 1 and 2). In these heatmaps, each cell

represents the thetaYC dissimilarity between two samples based on their zOTU composition. Values close to 0 indicate greater similarity, whereas values close to 1 indicate greater dissimilarity. In 2023, Bs alone showed greater bacterial similarity among replicates, and greater dissimilarity from most other treatments (Figure 1). UTC showed moderate within-treatment variability, while some replicates exhibited greater similarity than others. In 2024, Bs rotated with synthetics remained variable among replicates but showed high pairwise dissimilarity from most other treatments, whereas Bs alone exhibited comparatively stronger within-treatment similarity. UTC displayed comparatively stronger within-treatment similarity, suggesting a more consistent bacterial community among replicates, while showing high dissimilarity from most other treatments.

In 2023, fungal communities showed considerable within-treatment variability, particularly under Sl rotated with synthetic fungicides. The Sl-rotation treatment displayed replicate-to-replicate heterogeneity, with one replicate showing high dissimilarity. The UTC also showed variable fungal community compositions among replicates, including a highly dissimilar replicate. In 2024, substantial within-treatment variation persisted, especially for Sl rotated with synthetic fungicides, while several other treatments also showed inconsistent replicate clustering. Although some replicate pairs within the UTC were relatively similar in 2024, the UTC did not form a consistently distinct cluster. Overall, fungal communities showed considerable replicate-to-replicate variation in both years, indicating that treatment-associated fungal community patterns were weak and inconsistent (Figure 2).

3.3. Dominant Prokaryotic (Bacteria) Microbial Communities

According to the total relative abundance data, zOTUs putatively annotated as *Methylobacterium adhaesivum* (17.05%) from the phylum of Proteobacteria and class of Alphaproteobacteria, and *Bacillus velezensis* (11.4%) and *Staphylococcus pasteuri* (6.41%) from the phylum of Firmicutes and class of Bacilli, *Sediminibacterium salmoneum* (7.01%) from the phylum Bacteroidetes made up more than 40% of the entire bacterial community in 2023 (Figures 3 and 4). The remaining taxa were detected at moderate to low levels, with relative abundances ranging from 4.61% to 0.62% (Supplementary File S2). Within the Rs treatment, *Fructobacillus fructosus* was abundant in one high-depth replicate but was not detected in the remaining low-depth replicates; thus, it was not interpreted as treatment-level dominance. In Sl alone application, the bacterial community was led by *M. adhaesivum* (26%), while Sl rotated with synthetics resulted in 32.7%.

Bs and Bs rotated with synthetics were dominated by *B. velezensis* (46.5% and 43.5%, respectively), with *M. adhaesivum* also abundant when Bs was rotated with synthetics (23.2%). All synthetics were characterized primarily by *S. pasteuri* (16.8%), *Dietzia alimentaria* (15.1%), and *M. adhaesivum* (14.5%), whereas the untreated control was dominated by *M. adhaesivum* (10.9%) and *M. dankookense* (10.4%), followed by *Pseudomonas amygdali* (5.7%).

In 2024, the overall relative abundance data revealed a less skewed but nonetheless hierarchical community structure, zOTUs putatively annotated as *B. atrophaeus* (6.7%), *Bosea massiliensis* (6.29%), and *Hydrotalea flava* (6.01%) emerging as the three dominant species, followed by *X. cassavae* (3.36%), *Reyranella massiliensis* (2.57%), and *Ralstonia pickettii* (1.78%) while the majority of other taxa are present at relatively low abundances (<2%). Rs alone treatment was dominated by *Calycomorphotria hydatis* (9.01%), *Hydrotalea flava* (7.61%), followed by *Xanthomonas cassavae* (6.47%), whereas Rs rotated with synthetics was led by *H. flava* (12.1%), *Bosea massiliensis* (10.7%), and *X. cassavae* (3.38%). Sl alone treatment was overwhelmingly dominated by *Sporosarcina soli* (59.8%), whereas *Halomonas stevensii* (10.8%), *Erwinia mallotivora* (10.1%), and *X. cassavae* (5.03%) dominated the treatment with Sl rotated with synthetics. Bs alone and Bs rotated with synthetics were dominated by *B. atrophaeus* (7.47% and 23.7%, respectively). All synthetics and the untreated control were

dominated by *B. massiliensis* (7.72%) and *B. aerolatus* (9.61%), respectively, as the most abundant species.

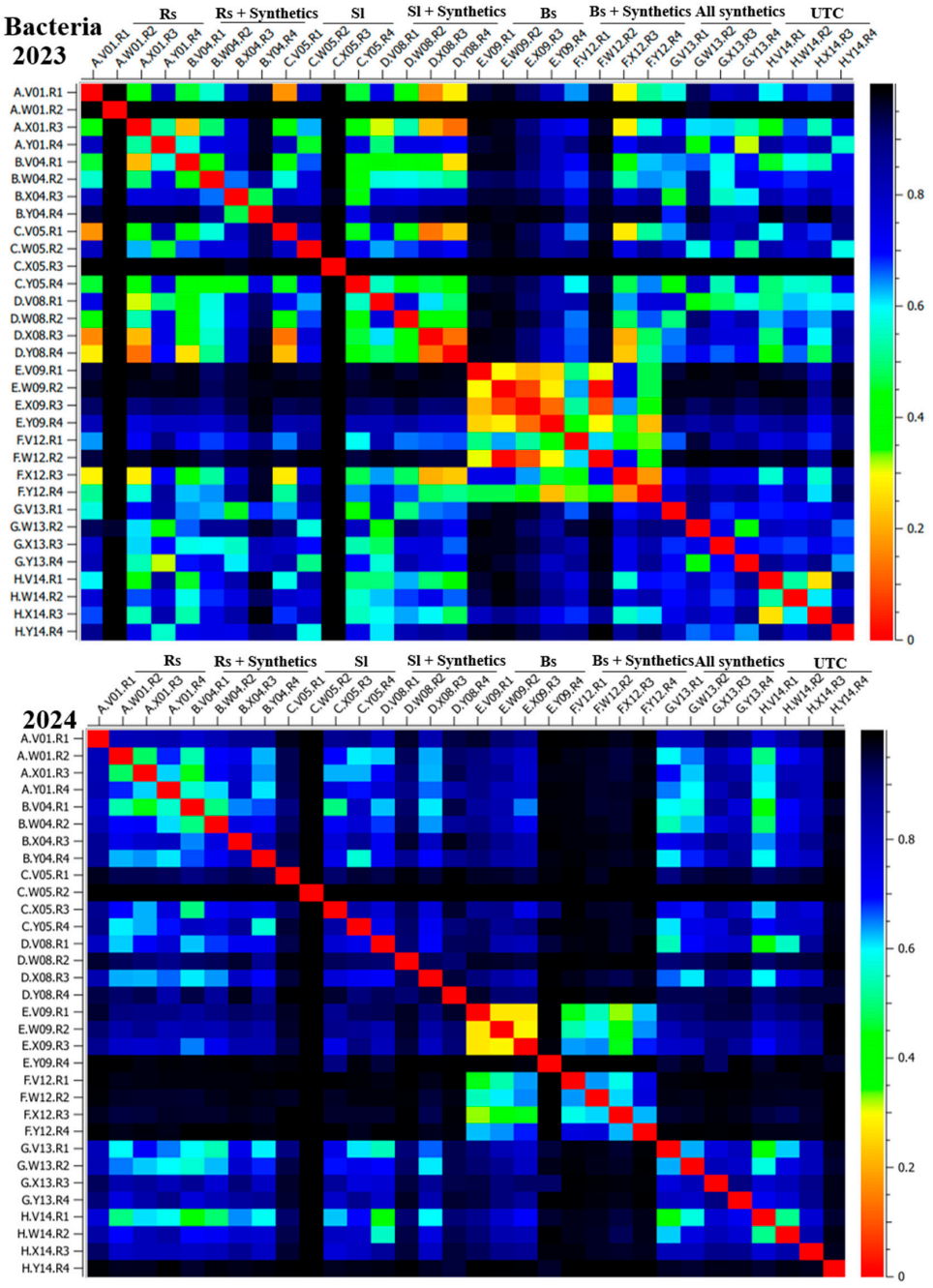


Figure 1. Pairwise bacterial community dissimilarity among grape berry surface samples collected in 2023 and 2024, calculated using the Yue–Clayton thetaYC metric. Each row and column represents one sample (n = 32 samples per year). Each cell shows the thetaYC dissimilarity value between two samples based on zOTU composition. Values close to 0 (red) indicate highly similar community composition, whereas values close to 1 (black) indicate greater community dissimilarity. Samples are grouped by treatment and replicate. Rs = Extract of *Reynoutria sachalinensis*, Sl = *Streptomyces lydicus*-based product, Bs = *Bacillus subtilis*-based product, UTC = Untreated Control.

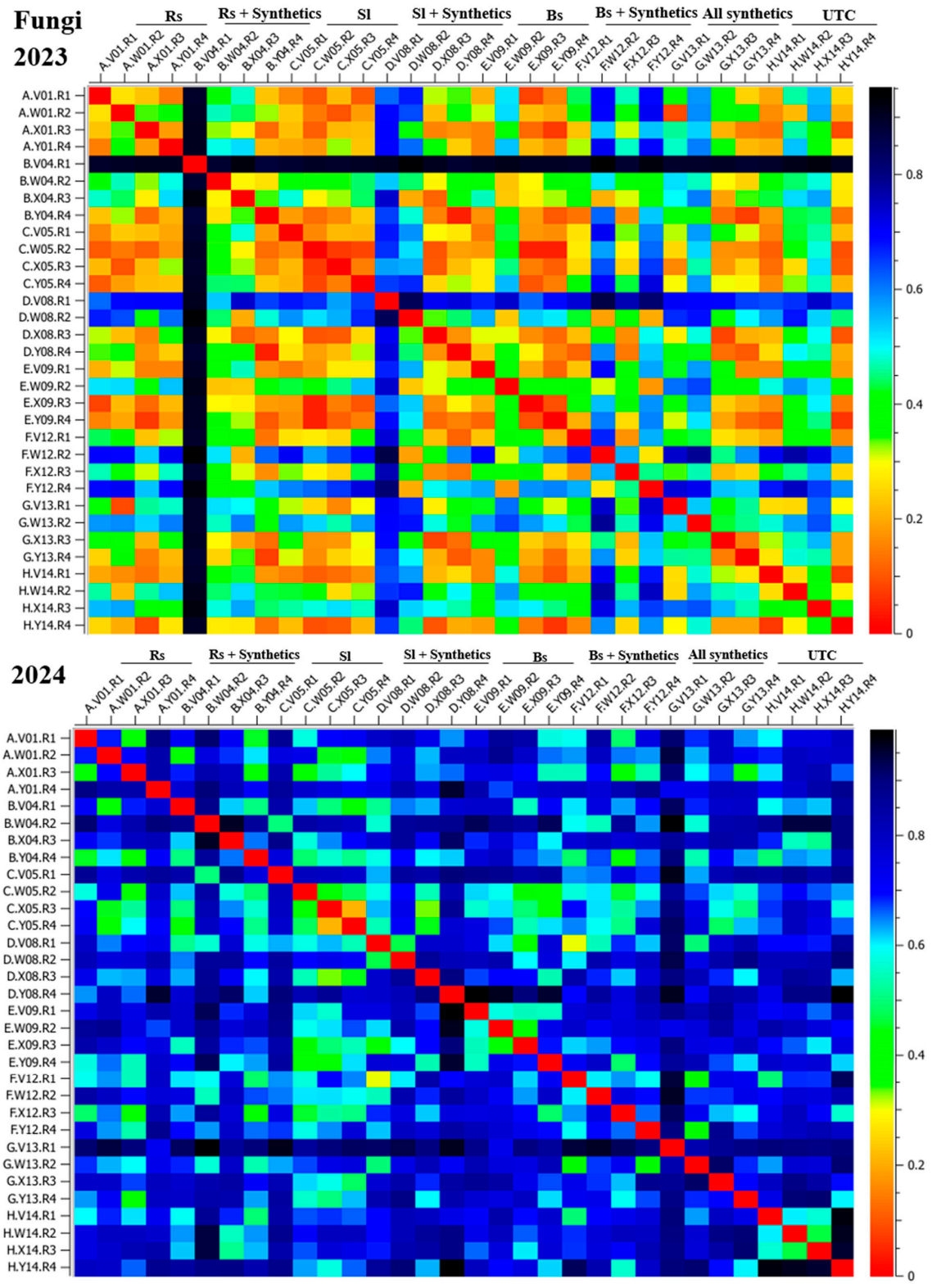


Figure 2. Pairwise fungal community dissimilarity among grape berry surface samples collected in 2023 and 2024, calculated using the Yue–Clayton thetaYC metric. Each row and column represents one sample (n = 32 samples per year). Each cell shows the thetaYC dissimilarity value between two samples based on fungal zOTU composition. Values close to 0 (red) indicate highly similar community composition, whereas values close to 1 (black) indicate greater community dissimilarity. Samples are grouped by treatment and replicate. Rs = Extract of *Reynoutria sachalinensis*, Sl = *Streptomyces lydicus*-based product, Bs = *Bacillus subtilis*-based product, UTC = Untreated Control.

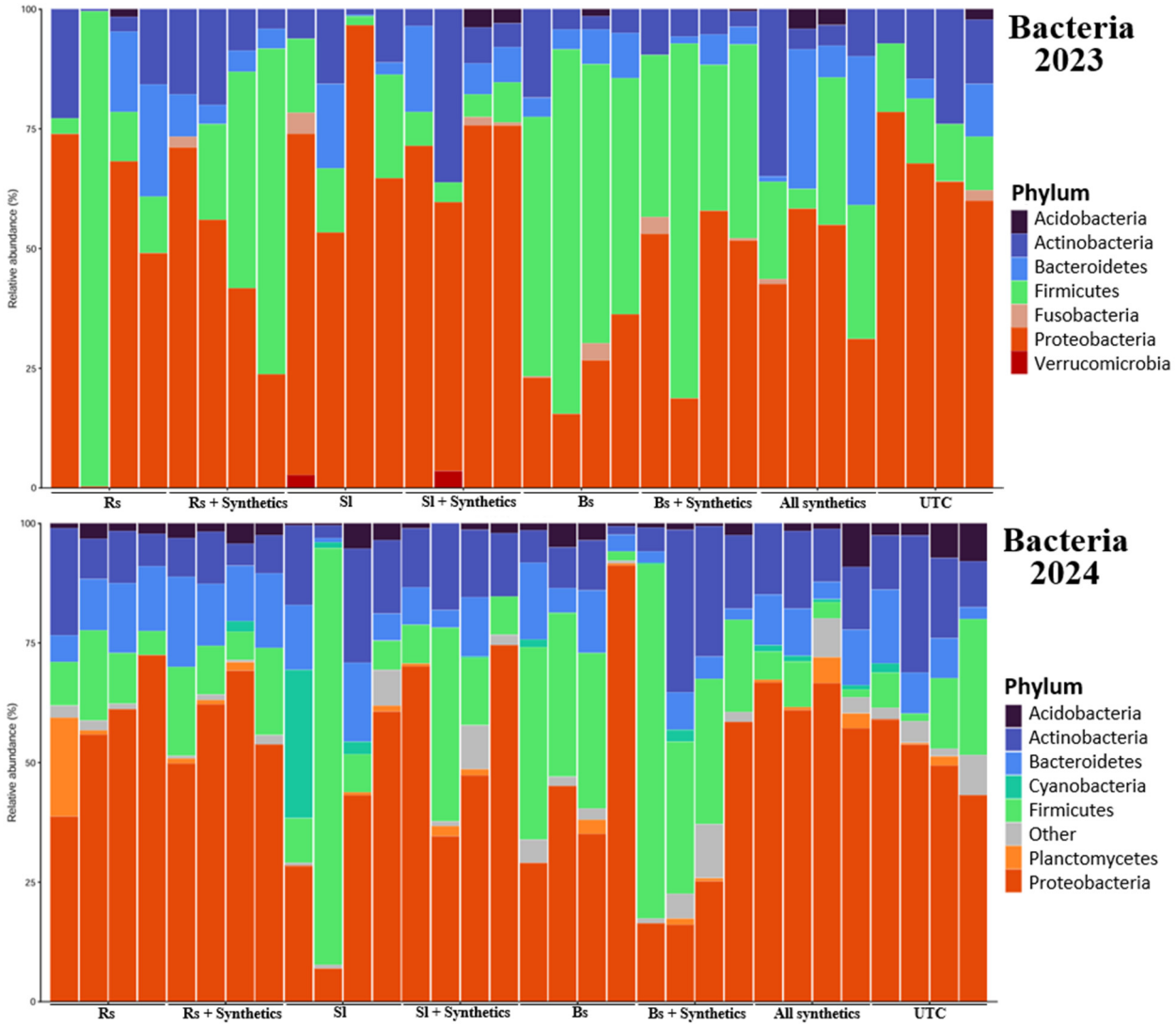


Figure 3. Relative abundances of bacterial communities (2023–2024) at the phylum level from the grape berry surface of different treatments. For each treatment, four stacked bars represent the four experimental plots (replicates), with different colors indicating the relative abundance (%) of bacterial phyla within each replicate. Rs = Extract of *Reynoutria sachalinensis*, Sl = *Streptomyces lydicus*-based product, Bs = *Bacillus subtilis*-based product, UTC = Untreated Control. Taxonomic labels were standardized using traditional nomenclature across both years. For the bacterial communities, phyla with a mean relative abundance of <1% across all samples were grouped as "Other".

3.4. Dominant Eukaryotic (Fungi) Microbial Communities

In 2023, overall relative-abundance data for fungal taxa showed that more than 50% of fungal reads were represented by zOTUs putatively annotated as *Cladosporium chasmanthicola* (16.49%), *C. puyae* (14.02%), and *C. herbarum* (11.78%) along with other *Cladosporium* spp. within the class Dothideomycetes under the phylum Ascomycota, and the nearest dominant *Aureobasidium leucospermi* (4.23%), within the same class and phylum (Figures 5 and 6). The moderate contributions like *Aspergillus xerophilus* (3.24%), *Cryptococcus carnescens* (3.0%), and *Clydaea vesicula* (2.89%) revealed a highly uneven distribution dominated by a few abundant fungal taxa, while the remaining species occurred at low relative abundances (<2%). At the treatment level, *C. chasmanthicola*, *C. puyae*, and *C. herbarum* were consistently dominant among all treatments. Other notable taxa including *Alternaria infectoria* (syn. *Lewia infectoria*) were present in all treatments, while zOTUs putatively annotated as the powdery mildew pathogen *Erysiphe necator* represented 0.36% and 0.30% in Sl and Bs alone

treatments, respectively. Botrytis bunch rot causal agent *Botrytis cinerea* (syn. *Botryotinia fuckeliana*) (2.07%) was observed in Sl alone treatment, whereas 5.67% was observed in UTC (Supplementary File S2).

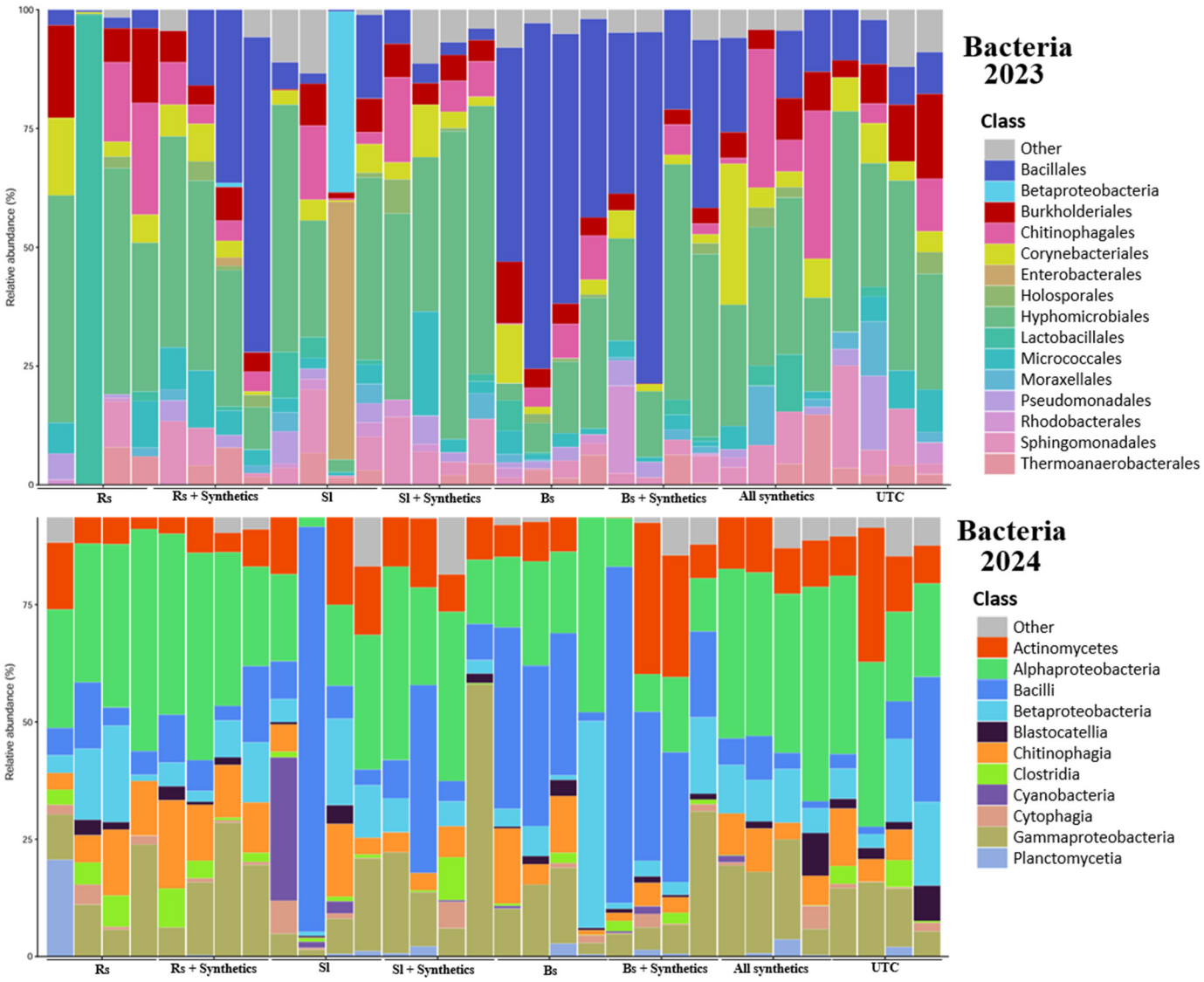


Figure 4. Relative abundances of bacterial communities (2023–2024) at the class level from the grape berry surface of different treatments. For each treatment, four stacked bars represent the four experimental plots (replicates), with different colors indicating the relative abundance (%) of bacterial classes within each replicate. Rs = Extract of *Reynoutria sachalinensis*, Sl = *Streptomyces lydicus*-based product, Bs = *Bacillus subtilis*-based product, UTC = Untreated Control. Taxonomic labels were standardized using traditional nomenclature across both years. For the bacterial communities, classes with a mean relative abundance of <1% across all samples were grouped as "Other".

In 2024, fungal zOTUs putatively annotated as *C. chasmanthicola* (38.01%), *C. puyae* (11.49%), and *C. herbarum* (8.30%) according to the overall relative abundance, followed by *Aureobasidium pullulans* (6.20%), *Alternaria infectoria* (5.03%), and *Erysiphe necator* (4.24%), with the rest of the species having low relative abundances. *C. chasmanthicola* was the most abundant species in every treatment, ranging from 29.3% in Sl rotated with synthetics to 44.7% in Rs alone treatment. Other commonly detected taxa included *Aureobasidium pullulans*, *Alternaria infectoria*, *Cryptococcus carnescens*, along with *Cladosporium* spp. from all treatments. The powdery mildew pathogen *Erysiphe necator* was particularly abundant

in Rs alone (11.3%) and Bs rotated with synthetics (14.4%), while it was 4.24% in UTC. The Botrytis bunch rot pathogen *Botrytis cinerea* was detected at low relative abundance, ranging from 0.25% to 1.56% in Sl and Rs alone treatments, respectively. Overall, the fungal communities showed an uneven distribution, with a few dominant *Cladosporium* taxa comprising most of the community and the remaining species occurring at relatively low abundances.

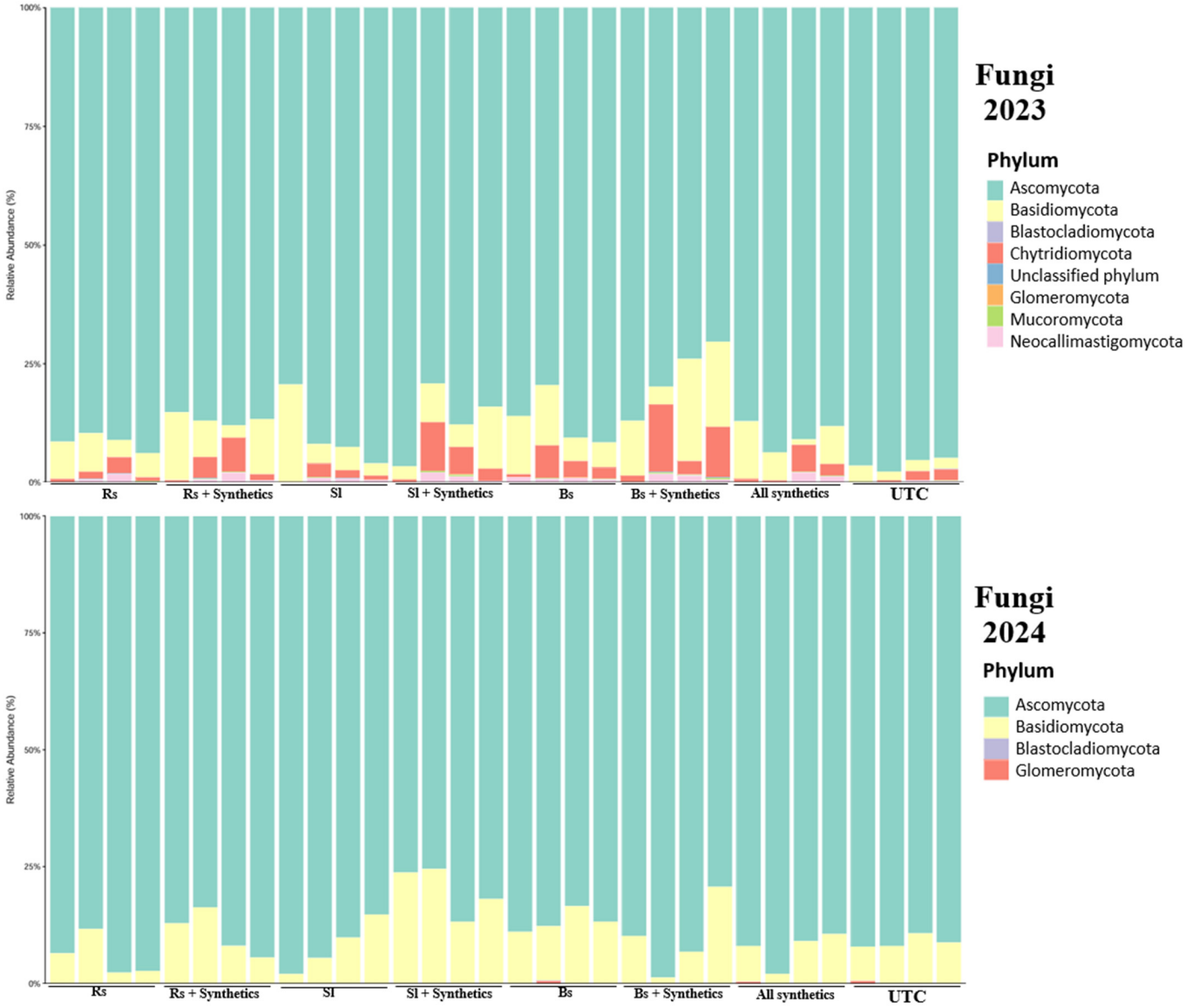


Figure 5. Relative abundances of fungal communities (2023–2024) at the phylum level from the grape berry surface of different treatments. For each treatment, four stacked bars represent the four experimental plots (replicates), with different colors indicating the relative abundance (%) of fungal phyla within each replicate. Rs = Extract of *Reynoutria sachalinensis*, Sl = *Streptomyces lydicus*-based product, Bs = *Bacillus subtilis*-based product, UTC = Untreated Control.

3.5. Beta Diversity Analysis (Bacteria)

The hierarchical clustering of the bacterial community showed similarity across treatments, and the similarity scale (0.2–1.0) indicated the degree of resemblance among treatment-associated communities, with values closer to 1.0 reflecting greater similarity (Figure 7A). In 2023, most treatments were concentrated near the center of the principal coordinates analyses (PCoA), indicating relatively similar microbial community composi-

tion, although several individual replicates, particularly from Rs alone, Bs alone, and Bs rotated with synthetics, were widely separated from the main group, indicating considerable within-treatment variability (Figure 7B). For the similarity index in 2023, Sl alone and Sl rotated with synthetics clustered closely with all synthetics, while Bs alone and Bs rotated with synthetics formed a separate similarity group; Rs rotated with synthetics and UTC also clustered together but were more differentiated from the remaining treatments.

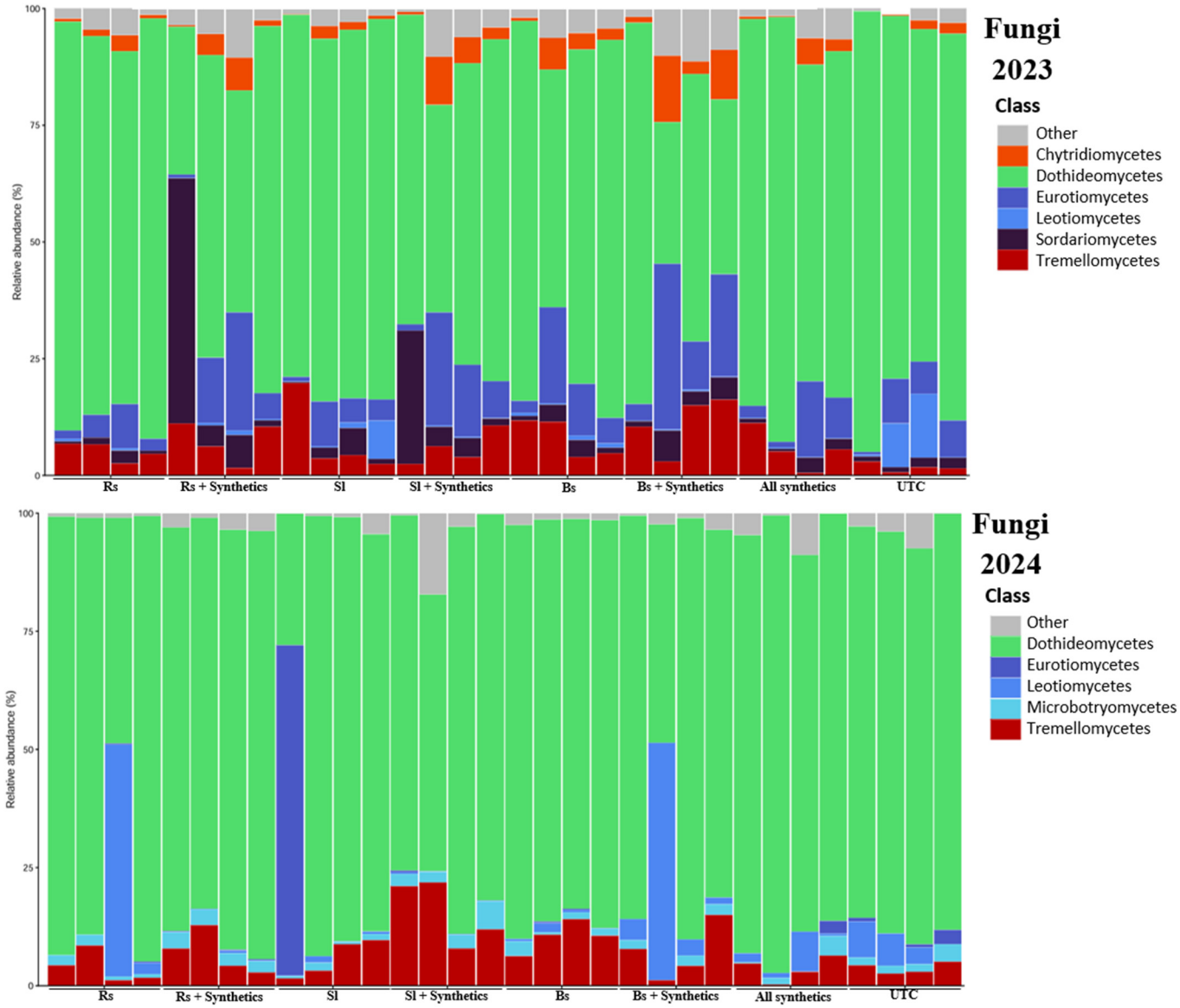


Figure 6. Relative abundances of fungal communities (2023–2024) at the class level from the grape berry surface of different treatments. For each treatment, four stacked bars represent the four experimental plots (replicates), with different colors indicating the relative abundance (%) of fungal classes within each replicate. Rs = Extract of *Reynoutria sachalinensis*, Sl = *Streptomyces lydicus*-based product, Bs = *Bacillus subtilis*-based product, UTC = Untreated Control. For the fungal communities, classes with a mean relative abundance of <1% across all samples were grouped as "Other".

In 2024, Rs alone and all synthetics grouped relatively closely, replicates from most treatments did not consistently cluster together, indicating considerable within-treatment variability and incomplete treatment-specific separation (Figure 7C). For the similarity index in 2024, the clustering structure changed, with Sl rotated with synthetics and Rs alone clustered together but close to the all synthetics treatment, while Sl alone, UTC, and Bs

alone formed another closely related group (Figure 7D). Bs rotated with synthetics showed the greatest separation from the other treatments. These variations indicated that treatment associated bacterial community relationships were not consistent between years.

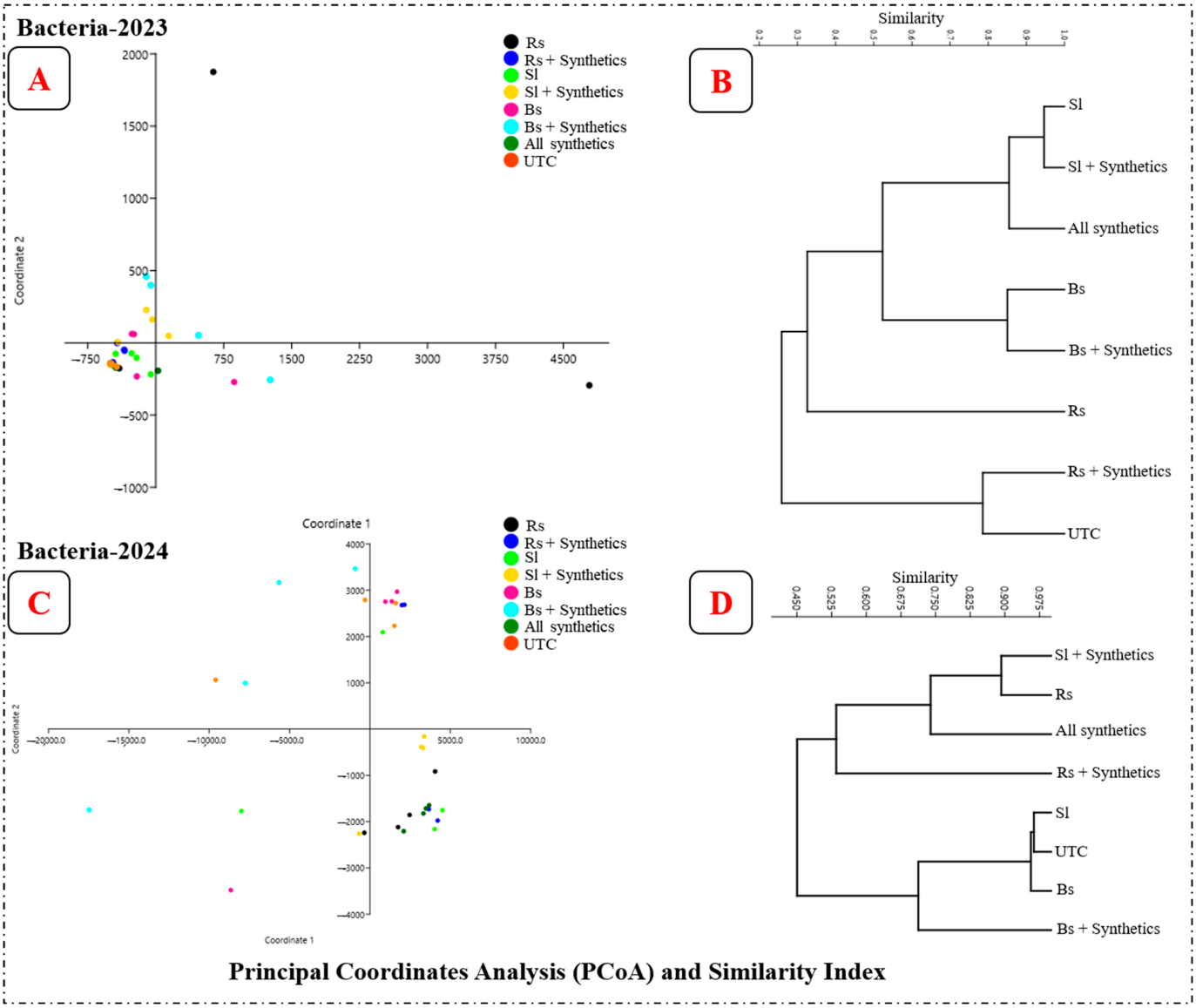


Figure 7. Principal coordinate analysis (**A**,**C**) based on Bray–Curtis dissimilarities and unweighted pair group method with arithmetic mean (UPGMA) clustering (**B**,**D**) of bacterial community composition across treatments. Each point represents one biological replicate sample ($n = 4$ per treatment; total $n = 32$ samples per year). Rs = Extract of *Reynoutria sachalinensis*, Sl = *Streptomyces lydicus*-based product, Bs = *Bacillus subtilis*-based product, UTC = Untreated Control.

3.6. Beta Diversity Analysis (Fungi)

In 2023, the PCoA plot showed substantial overlap among fungal communities from the different treatment programs, although several individual samples were separated from the main group, indicating within-treatment variability (Figure 8A). The similarity scale (0.8–0.98) indicates how closely microbial profiles resemble one another, with higher values showing greater overlap. The UPGMA dendrogram showed that Rs alone and Rs rotated with synthetic fungicides were the most similar treatments. Bs rotated with synthetic fungicides and the all synthetics treatment also formed a closely related cluster, whereas UTC was separated from the other treatment groups at a lower similarity level (Figure 8B).

In 2024, the PCoA plot again showed overlap among many treatment groups, with several samples positioned away from the central cluster, indicating variability in fungal community composition among replicates (Figure 8C). The similarity scale (0.99–1.0) indicates how closely microbial profiles resemble one another, with higher values showing greater overlap. In 2024, the UPGMA dendrogram displayed a narrow similarity-axis range (0.99–1.00). Because this compressed scale limits interpretation of small branch-length differences, the dendrogram was used only to visualize clustering patterns and not to infer meaningful quantitative differences in fungal community similarity among treatments. The UPGMA dendrogram showed a close association between Rs alone and Rs rotated with synthetic fungicides, with Sl alone and Sl rotated with synthetic fungicides joining this broader cluster (Figure 8D). In contrast, the all synthetics treatment and UTC formed a separate cluster, indicating that their fungal community profiles were more similar to each other than to the remaining treatment programs.

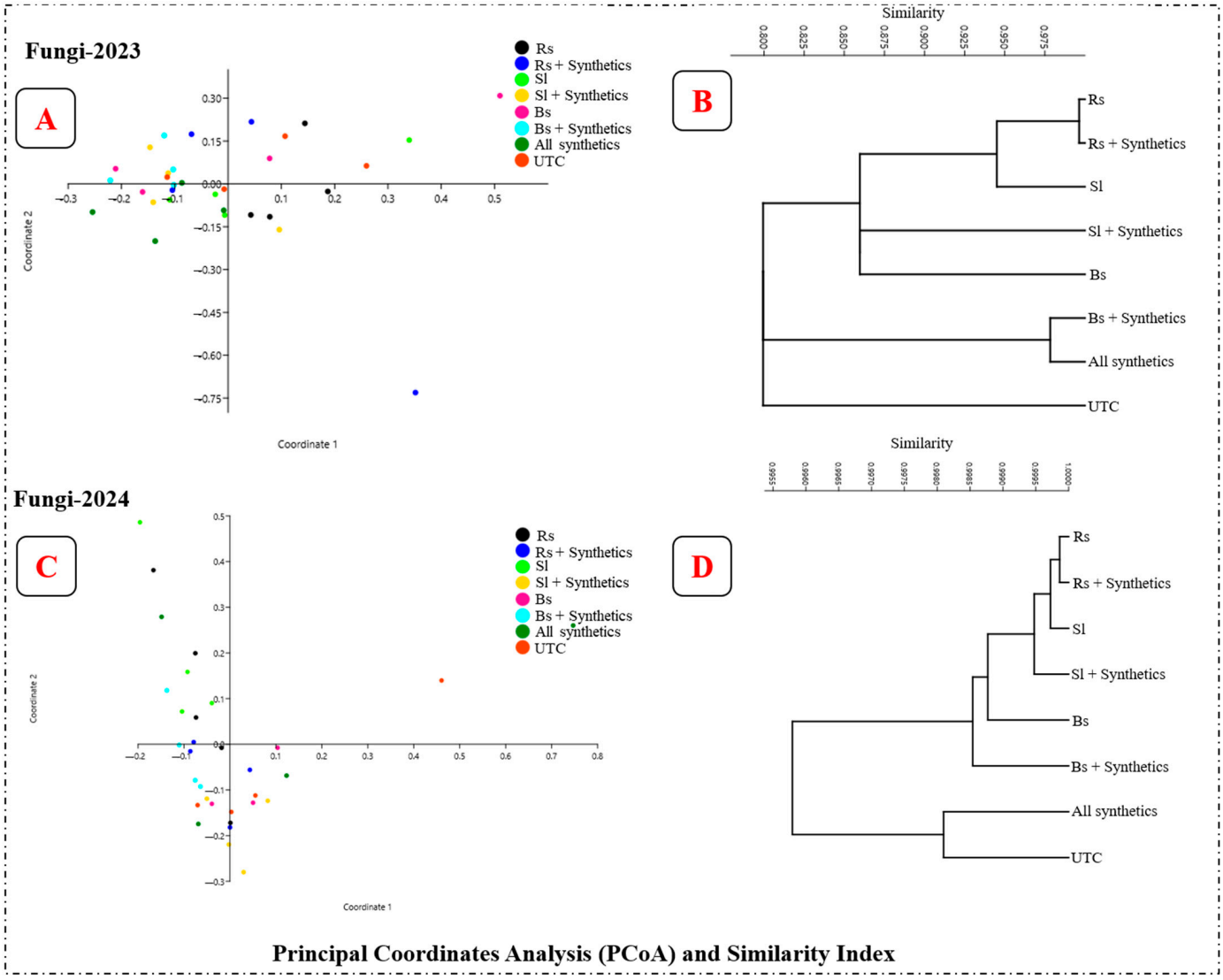


Figure 8. Principal coordinate analysis (**A**,**C**) based on Bray–Curtis dissimilarities and unweighted pair group method with arithmetic mean (UPGMA) clustering (**B**,**D**) of fungal community composition across treatments. Each point represents one biological replicate sample (n = 4 per treatment; total n = 32 samples per year). Rs = Extract of *Reynoutria sachalinensis*, Sl = *Streptomyces lydicus*-based product, Bs = *Bacillus subtilis*-based product, UTC = Untreated Control.

3.7. Multivariate Treatment Effects (PERMANOVA and PERMDISP)

PERMANOVA based on Bray–Curtis dissimilarities indicated significant treatment-associated differences in bacterial and fungal community composition after accounting for block effects (Table 2). For bacterial communities, treatment explained 36.2% of compositional variation in 2023 (*pseudo-F* = 2.030, $p = 0.0001$) and 30.8% in 2024 (*pseudo-F* = 1.533, $p = 0.0001$). For fungal communities, treatment accounted for 32.5% of variation in 2023 (*pseudo-F* = 1.946, $p = 0.0011$) and 31.2% in 2024 (*pseudo-F* = 1.550, $p = 0.0106$). PERMDISP tests were not significant for bacterial communities in 2023 ($F = 1.036$, $p = 0.3521$) or 2024 ($F = 1.014$, $p = 0.1131$), or for fungal communities in 2023 ($F = 0.749$, $p = 0.4212$) or 2024 ($F = 0.508$, $p = 0.8780$). Thus, the PERMANOVA results were not attributable to unequal multivariate dispersion among treatments. However, PCoA and clustering analyses showed replicate-level variation and treatment overlap; therefore, the results indicate treatment-associated compositional differences rather than complete separation of treatment groups. The 2023 bacterial results should be interpreted cautiously because sequencing depth was low and highly variable among samples. Although PERMANOVA detected overall treatment-associated compositional differences, PCoA and UPGMA analyses showed substantial replicate-level variation and overlap among treatments; therefore, the results do not indicate complete or consistent treatment-specific clustering.

Table 2. PERMANOVA and PERMDISP results for effects of fungicide treatments on bacterial and fungal communities on "Pinot Noir" berry surfaces.

Community	Year	PERMANOVA *Pseudo-F*	PERMANOVA R^2	PERMANOVA *p*	PERMDISP *F*	PERMDISP *p*
Bacteria	2023	2.030	0.362	0.0001	1.036	0.3521
	2024	1.533	0.308	0.0001	1.014	0.1131
Fungi	2023	1.946	0.325	0.0011	0.749	0.4212
	2024	1.550	0.312	0.0106	0.508	0.8780

Note: Each analysis included 32 samples ($n = 32$). Bray–Curtis dissimilarities were calculated from relative-abundance-transformed zOTU count data. PERMANOVA models included Block (df = 3) and Treatment (df = 7), with treatment effects evaluated after accounting for block; residual df = 21. Analyses were conducted separately for each year and community type using 9999 permutations restricted within blocks. PERMDISP tested homogeneity of multivariate dispersion among treatments using the same distance matrices. PERMANOVA models were fitted as Block + Treatment, and the reported treatment statistics were calculated after accounting for Block. Pairwise PERMANOVA tests were not conducted; therefore, no inference was made regarding differences between specific treatment pairs.

3.8. Alpha Diversity Analysis (Bacteria)

In 2023, bacterial Chao1 richness ranged from 23.67 under all synthetics treatment to 46.08 under Sl alone, while Shannon diversity ranged from 1.89 under Rs alone to 2.65 in the UTC (Table 3). After accounting for experimental block, neither Chao1 richness nor Shannon diversity differed significantly among treatments (Chao1, $p = 0.200$; Shannon, $p = 0.567$). In 2024, Chao1 richness ranged from 51.00 under Sl rotated with synthetics to 90.59 in the UTC, whereas Shannon diversity ranged from 2.89 under Sl alone to 3.80 in the UTC. After accounting for block, no significant treatment effects were detected for Chao1 richness ($p = 0.399$) or Shannon diversity ($p = 0.234$). Given the low and uneven bacterial sequencing depth in 2023, alpha-diversity results were interpreted separately within each year, and no between year comparison was made.

Table 3. Chao1 richness and Shannon diversity of bacterial communities by treatment in 2023 and 2024.

Year	Diversity Indices	Rs	Rs + Synthetics	Sl	Sl + Synthetics	Bs	Bs + Synthetics	All Synthetics	UTC	Block-Adjusted *p*-Value
2023	Chao1	25.67 ± 8.60	30.80 ± 5.52	46.08 ± 27.24	27.54 ± 6.58	33.54 ± 8.65	27.65 ± 5.07	23.67 ± 7.38	26.69 ± 4.95	0.200
	Shannon	1.89 ± 0.89	2.36 ± 0.56	2.32 ± 0.66	2.48 ± 0.24	2.05 ± 0.46	2.05 ± 0.53	2.42 ± 0.21	2.65 ± 0.44	0.567
2024	Chao1	58.45 ± 16.75	61.53 ± 12.37	78.83 ± 24.61	51.00 ± 15.03	76.15 ± 35.42	86.35 ± 35.35	81.17 ± 43.40	90.59 ± 24.56	0.399
	Shannon	3.38 ± 0.29	3.31 ± 0.13	2.89 ± 1.19	3.32 ± 0.32	3.01 ± 0.29	2.91 ± 0.94	3.64 ± 0.17	3.80 ± 0.23	0.234

Note: Rs = Extract of *Reynoutria sachalinensis*, Sl = *Streptomyces lydicus*-based product, Bs = *Bacillus subtilis*-based product, UTC = Untreated Control. Values are presented as mean ± SD (n = 4). Treatment effects were assessed separately for each year's dataset using a randomized complete block design with restricted permutation tests (9999 permutations).

3.9. Alpha Diversity Analysis (Fungi)

Fungal Chao1 richness and Shannon diversity varied numerically among treatments (Table 4). However, in 2023, the all synthetics treatment had the numerically lowest Chao1 richness (148.39) and lowest Shannon diversity (2.58), whereas Bs applied alone had the highest Chao1 richness (174.52), and Bs rotated with synthetic fungicides had the highest Shannon diversity (3.07) (Table 4). In 2024, fungal Chao1 richness was numerically lowest under Bs applied alone (104.48) and highest under Rs applied alone (145.96). UTC showed the numerically highest Shannon diversity (2.33), whereas Sl applied alone showed the lowest Shannon diversity (1.80). After accounting for experimental block, neither Chao1 richness nor Shannon diversity differed significantly among treatments in 2023 (Chao1, $p = 0.094$; Shannon, $p = 0.230$). In 2024, Chao1 richness did not differ among treatments ($p = 0.996$), whereas Shannon diversity showed a marginal overall treatment effect ($F_{7,21} = 2.53$, restricted-permutation $p = 0.047$). This result should be interpreted cautiously. Fungal alpha-diversity results were also interpreted separately within each year; no formal between-year comparisons were performed.

Table 4. Chao1 richness and Shannon diversity of fungal communities by treatment in 2023 and 2024.

Year	Diversity Indices	Rs	Rs + Synthetics	Sl	Sl + Synthetics	Bs	Bs + Synthetics	All Synthetics	UTC	Block-Adjusted *p*-Value
2023	Chao1	169.98 ± 11.04	164.14 ± 21.02	172.27 ± 25.33	157.21 ± 15.30	174.52 ± 26.44	164.54 ± 21.91	148.39 ± 21.02	156.88 ± 23.71	0.094
	Shannon	2.62 ± 0.28	2.80 ± 0.62	2.60 ± 0.13	2.82 ± 0.50	2.93 ± 0.25	3.07 ± 0.30	2.58 ± 0.33	2.67 ± 0.25	0.230
2024	Chao1	145.96 ± 101.42	112.21 ± 19.07	105.36 ± 6.38	114.28 ± 27.73	104.48 ± 8.94	111.55 ± 28.38	130.36 ± 78.15	105.99 ± 47.50	0.996
	Shannon	1.86 ± 0.40	2.16 ± 0.24	1.80 ± 0.36	2.28 ± 0.07	2.32 ± 0.07	2.01 ± 0.18	2.06 ± 0.35	2.33 ± 0.17	0.047

Note: Rs = Extract of *Reynoutria sachalinensis*, Sl = *Streptomyces lydicus*-based product, Bs = *Bacillus subtilis*-based product, UTC = Untreated Control. Values are presented as mean ± SD (n = 4). Treatment effects were assessed separately for each year's dataset using a randomized complete block design with restricted permutation tests (9999 permutations).

4. Discussion

In this study, we explored microbial communities on berry surfaces of "Pinot Noir" grape from the Central Coast region of California using amplicon-based microbiome profiling approaches. Bacterial community patterns were evaluated separately within each growing season because the low and uneven sequencing depth in 2023 precluded direct comparison with the 2024 bacterial dataset. For the bacterial communities, *Bacillus velezensis*

and *B. atrophaeus* showed high relative abundance when applied in Bs treatments in 2023 and 2024, respectively. Isolates of these *Bacillus* species have previously been reported to possess traits associated with pathogen antagonism, including biofilm formation and lipopeptide production [23]. *Bacillus* taxa have been reported previously from mature grape berries [35], and some isolates have been investigated for biocontrol- or plant-associated traits [36–39]. However, the present amplicon-sequencing data do not demonstrate that the detected *Bacillus* taxa expressed these traits or contributed to disease suppression in this vineyard. Because Bs is a *Bacillus*-based product, the high relative abundance of sequences assigned to *Bacillus* species in Bs-treated samples may reflect the applied product or closely related indigenous taxa. Although sequences were assigned at the species level, the 16S rRNA amplicon data did not provide strain-level resolution; therefore, establishment of the applied strain could not be confirmed. *B. velezensis* was detected in Bs-treated plots; however, this detection may reflect the applied Bs-based product rather than enrichment of an indigenous beneficial taxon. *Streptomyces lydicus* was not detected in Sl-treated plots, although other *Streptomyces* spp. were detected. *Methylobacterium adhaesivum* showed high relative abundance in Sl-treated samples from our study. Members of *Methylobacterium* are frequently associated with grapevine phyllospheres, and some isolates have previously been reported to possess plant-associated traits, including phytohormone production [40,41].

Several fungal taxa were detected across treatments and years, although their relative representation varied between years. For the fungal communities, *Cladosporium puyae*, *C. herbarum*, and *C. chasmanthicola* were among the most frequently detected fungal taxa across treatments in 2023, whereas *C. chasmanthicola* had high relative abundance across treatments in 2024. In addition, several *Cladosporium* spp. including *C. colombiae*, *C. herbarum*, and *C. puyae* were observed under certain conditions in both years. *Cladosporium* spp. are frequently reported as saprophytic or opportunistic fungi in vineyards worldwide [13]. *Aureobasidium* spp. were detected from both years of fungicide application. Previously recognized as major members of the grape epidermis, the genera of *Aureobasidium*, *Cladosporium*, and *Alternaria* were shown to peak at harvest [42–46], with *Aureobasidium* and *Alternaria* genera becoming dominant when berries were maturing [35]. Similarly, Nardi et al. reported that *Aureobasidium pullulans* was the most prevalent species on grape surfaces in an Italian vineyard study, whereas *Hanseniaspora uvarum*, *C. ramotenellium*, *C. cladosporioides*, *Zygosaccharomyces rouxii*, and *Starmerella bacillaris* were also detected in lower abundances [46]. Isolates of *Aureobasidium* have previously been investigated for antagonistic activity against phyllosphere and postharvest pathogens [10]; however, the present data do not demonstrate such activity in the sampled vineyard.

Fungal community composition differed between 2023 and 2024, with changes in the dominant fungal zOTUs between years. These year-to-year differences may reflect unmeasured vintage-related factors, such as environmental conditions, berry phenology, or differences in background inoculum. However, seasonal variables were not analyzed in this study; therefore, the effects of specific seasonal conditions on fungal community composition cannot be determined. In addition, the different ITS read lengths used in 2023 and 2024 represent a technical year effect and should be considered when interpreting between-year fungal community differences. This variability may reflect the role of *Reynoutria sachalinensis* as a plant-defense elicitor rather than a direct microbial antagonist; however, this explanation remains hypothetical because host-defense responses and plant metabolites were not measured [20]. Fungicide programs were associated with differences in the relative representation of bacterial and fungal taxa; however, the data do not establish pathogen suppression or recruitment of functionally beneficial microorganisms. The fungicide programs in this study were targeted at managing grapevine powdery mildew, which is caused by *Erysiphe necator*. Disease incidence and severity were not formally as-

sessed; therefore, no conclusions regarding disease risk or fungicide efficacy can be drawn. Sequences assigned to *E. necator* were detected in the untreated control in both years and in some Sl- and Bs-treated samples. The absence of detected *E. necator* sequences in other samples does not confirm that the pathogen was absent or indicate disease suppression. Additional taxa belonging to *Cladosporium* and *Alternaria* were detected. Some species within these genera have previously been associated with grape diseases. *Alternaria infectoria* was detected from treatments with Rs alone and Bs alone in 2023, and subsequently observed with the treatments of Rs alone, Sl alone, and UTC in 2024. *A. infectoria* on grapes is generally opportunistic, which may cause Alternaria bunch rot in ripening or injured berries [47,48].

Several taxa detected in Bs- and Sl-treated samples have previously been associated with biocontrol or plant-associated functions in other studies. These treatment-associated compositional patterns are consistent with reports that vineyard management may influence microbial community structure [9,10]. For example, Burns et al. found that vineyard bacterial communities were structured by management practices including cover crop, tillage, and production system [17]. This study has several limitations that should be considered when interpreting the results. The microbial community study was conducted at a single vineyard site with four biological replicates per treatment, with samples collected approximately one week prior to commercial maturity; therefore, the findings may not represent all vineyards, seasons, or production systems. In addition, amplicon sequencing provides compositional, DNA-based relative-abundance information and cannot determine absolute microbial population sizes. Therefore, observed differences among treatments should be interpreted as shifts in relative taxonomic representation or community composition, rather than absolute increases or decreases in microbial populations. Amplicon sequencing cannot determine whether detected taxa were viable, metabolically active, capable of causing disease, or expressing biocontrol or plant-growth-promotion traits; therefore, pathogen-associated taxa should be interpreted cautiously. A limitation of this study is that the methylene chloride–Tris buffer recovery procedure was not compared with conventional grape-surface microbiome recovery methods, such as isotonic-buffer washing with a non-ionic surfactant. Therefore, potential differential detachment, lysis, or loss of particular bacterial or fungal taxa cannot be excluded. The results should consequently be interpreted as treatment-associated differences in microbial communities recovered using the present extraction procedure, rather than as a fully unbiased representation of all microorganisms present on grape berry surfaces. Most alpha-diversity tests were not significant; however, fungal Shannon diversity in 2024 showed a marginal overall treatment effect ($p = 0.047$), which should be interpreted cautiously. With only four biological replicates per treatment and lower sequencing depth in 2023, the power to detect moderate treatment effects and rare taxa was limited. Therefore, these findings should be interpreted cautiously, and future studies should include greater replication and balanced sequencing depth. Moreover, samples were collected at a single time point in each year, precluding assessment of temporal changes in berry-surface microbial communities. In addition, disease incidence or severity, yield, and fruit-quality parameters were not analyzed in this study; therefore, the relationships between treatment-associated microbiome patterns and disease-control performance or agronomic outcomes could not be determined.

5. Conclusions

This two-year study compared the effects of synthetic fungicides and biofungicides on the grape berry surface microbiomes of "Pinot Noir" grapes grown on the Central Coast of California. PERMANOVA indicated that treatment programs were associated with significant differences in bacterial and fungal community composition both in 2023 and 2024. Alpha-diversity metrics were generally not different among treatments; however, fungal

Shannon diversity in 2024 showed a marginal overall treatment effect. The proportion of compositional variation explained by treatment was broadly comparable between bacterial and fungal communities. Because microbial function, disease incidence and severity, yield, and fruit-quality parameters were not measured, the functional and agronomic implications of these treatment-associated microbiome shifts cannot be determined. Future research should evaluate how seasonal conditions, canopy microclimates, and fungicide rotation schedules influence microbial community dynamics and their relationships with disease pressure, fruit quality, and long-term vineyard sustainability.

Supplementary Materials: The following supporting information can be downloaded at: https://www.mdpi.com/article/10.3390/microorganisms14112676/s1. Supplementary File S1: Fungicide application dates, product rotations, active ingredients, application rates, and numbers of applications for all treatment programs in 2023 and 2024. Supplementary File S2: Microbial zOTU count matrices and sequencing-read statistics for bacterial and fungal communities associated with Pinot Noir berry surfaces in 2023 and 2024. The Excel workbook contains five worksheets: Bacterial zOTU-2023, Bacterial zOTU-2024, Fungal zOTU-2023, Fungal zOTU-2024, and Sequencing-read statistics, which reports raw paired-end and final retained reads for each sample. Figure S1: Rarefaction curves for bacterial and fungal zOTU datasets, showing observed zOTU richness as a function of sequencing depth for each biological replicate.

Author Contributions: Conceptualization, K.D. and S.D.; methodology, K.D. and S.D.; software, K.D. and S.S.H.; validation, K.D. and S.D.; formal analysis, K.D.; investigation, S.D.; resources, E.G.M., S.Z. and S.S.H.; data curation, K.D. and S.D.; writing—original draft preparation, K.D.; writing—review and editing, E.G.M., S.Z., S.S.H. and S.D.; visualization, K.D.; supervision, S.D.; funding acquisition, S.D. All authors have read and agreed to the published version of the manuscript.

Funding: The project was funded by the CDFA Specialty Crop Block Grant Program (Grant No. 22-0001-041-SF) and CSU-ARI (Project No. 23-01-101).

Institutional Review Board Statement: Not applicable.

Informed Consent Statement: Not applicable.

Data Availability Statement: The raw sequencing reads generated in this study have been deposited in the NCBI Sequence Read Archive (SRA) under the BioProject accession number PRJNA1518189. R scripts used for alpha-diversity, relative-abundance, and PERMANOVA analyses are publicly available through Zenodo at https://doi.org/10.5281/zenodo.23524336.

Acknowledgments: We thank Jim Green, Evan Tamayo, and Abraham Ahumada for supporting the fungicide spraying program.

Conflicts of Interest: The authors declare no conflicts of interest.

References

1. Wicaksono, W.A.; Morauf, C.; Müller, H.; Abdelfattah, A.; Donat, C.; Berg, G. The mature phyllosphere microbiome of grapevine is associated with resistance against *Plasmopara viticola*. *Front. Microbiol.* **2023**, *14*, 1149307. [CrossRef] [PubMed]
2. Africa, A.J.; Setati, M.E.; Hitzeroth, A.C.; Blancquaert, E.H. Exploring the evolution of microbial communities from the phyllosphere and carposphere to the grape must of *Vitis vinifera* L. cvs. Chardonnay and Pinot Noir. *Food Microbiol.* **2025**, *130*, 104780. [CrossRef] [PubMed]
3. Bokulich, N.A.; Thorngate, J.H.; Richardson, P.M.; Mills, D.A. Microbial biogeography of wine grapes is conditioned by cultivar, vintage, and climate. *Proc. Natl. Acad. Sci. USA* **2014**, *111*, E139–E148. [CrossRef] [PubMed]
4. Belda, I.; Zarraonaindia, I.; Perisin, M.; Palacios, A.; Acedo, A. From vineyard soil to wine fermentation: Microbiome approximations to explain the "terroir" concept. *Front. Microbiol.* **2017**, *8*, 821. Erratum in *Front. Microbiol.* **2017**, *8*, 1065. https://doi.org/10.3389/fmicb.2017.01065. [CrossRef] [PubMed]
5. Hed, B.; Centinari, M. Mechanical leaf removal for improved Botrytis bunch rot control in *Vitis vinifera* 'Pinot Gris' and 'Pinot Noir' grapevines in the northeastern United States. *Plant Dis.* **2024**, *108*, 3156–3162. [CrossRef] [PubMed]
6. Bettenfeld, P.; Fontaine, F.; Trouvelot, S.; Fernandez, O.; Courty, P.-E. Woody plant declines: What's wrong with the microbiome? *Trends Plant Sci.* **2020**, *25*, 381–394. [CrossRef] [PubMed]

7. Minerdi, D.; Sabbatini, P. Exploring the grapevine microbiome: Insights into the microbial ecosystem of grape berries. *Microorganisms* **2025**, *13*, 438. [CrossRef] [PubMed]
8. Zarraonaindia, I.; Owens, S.M.; Weisenhorn, P.; West, K.; Hampton-Marcell, J.; Lax, S.; Gilbert, J.A.; Bokulich, N.A.; Mills, D.A.; Martin, G.; et al. The soil microbiome influences grapevine-associated microbiota. *mBio* **2015**, *6*, e02527-14. [CrossRef] [PubMed]
9. Griggs, R.G.; Steenwerth, K.; Mills, D.A.; Bokulich, N.A. Sources and assembly of vineyard microbial communities. *mSystems* **2021**, *6*, e00516-20. [CrossRef] [PubMed]
10. Di Francesco, A.; Mari, M.; Neri, F. Microbial antagonists against in postharvest pathogens of stone fruit. *Postharvest Biol. Technol.* **2016**, *122*, 31–38. [CrossRef]
11. Grossi, C.E.M.; Ulloa, R.M.; Sahin, N.; Tani, A. Methylobacterium as a key symbiont in plant–microbe interactions: Its ecological and agricultural significance. *Plant Biotechnol.* **2025**, *42*, 229–241. [CrossRef] [PubMed]
12. Nimsi, K.A.; Manjusha, K.; Kathiresan, K.; Arya, H. Plant growth-promoting yeasts (PGPY), the latest entrant for use in sustainable agriculture: A review. *J. Appl. Microbiol.* **2023**, *134*, lxac088. [CrossRef] [PubMed]
13. Pinto, C.; Pinho, D.; Sousa, S.; Pinheiro, M.; Egas, C.; Gomes, A.C. Unravelling the diversity of grapevine microbiome. *PLoS ONE* **2014**, *9*, e85622. [CrossRef] [PubMed]
14. Gadoury, D.M.; Cadle-Davidson, L.; Wilcox, W.F.; Dry, I.B.; Seem, R.C.; Milgroom, M.G. Grapevine powdery mildew (*Erysiphe necator*): A fascinating system for the study of the biology, ecology and epidemiology of an obligate biotroph. *Mol. Plant Pathol.* **2012**, *13*, 1–16. [CrossRef] [PubMed]
15. Elmer, P.A.G.; Michailides, T.J. Epidemiology of *Botrytis cinerea* in orchard and vine crops. In *Botrytis: Biology, Pathology and Control*; Elad, Y., Williamson, B., Tudzynski, P., Delen, N., Eds.; Springer: Dordrecht, The Netherlands, 2004; pp. 243–272. [CrossRef]
16. Fedele, G.; Brischetto, C.; Rossi, V. Biocontrol of *Botrytis cinerea* on grape berries as influenced by temperature, relative humidity and colonization period of BCAs. *Front. Plant Sci.* **2020**, *11*, 1232. [CrossRef] [PubMed]
17. Burns, K.N.; Bokulich, N.A.; Cantu, D.; Greenhut, R.F.; Kluepfel, D.A.; O'Geen, A.T.; Strauss, S.L.; Steenwerth, K.L. Vineyard soil bacterial diversity and composition revealed by 16S rRNA genes: Differentiation by vineyard management. *Soil Biol. Biochem.* **2016**, *103*, 337–348. [CrossRef]
18. You, Z.; Zhuang, K.; Sugita, T.; Ran, Y. Novel Strategies against Fungal Infections: Repurposing Existing Drugs and Advancing Nanotherapeutics. *iFungi* **2026**. [CrossRef]
19. Pertot, I.; Caffi, T.; Rossi, V.; Mugnai, L.; Hoffmann, C.; Grando, M.S.; Gary, C.; Lafond, D.; Duso, C.; Thiery, D.; et al. A critical review of plant protection tools for reducing pesticide use on grapevine and new perspectives for the implementation of IPM in viticulture. *Crop Prot.* **2017**, *97*, 70–84. [CrossRef]
20. Margaritopoulou, T.; Toufexi, E.; Kizis, D.; Balayiannis, G.; Anagnostopoulos, C.; Theocharis, A.; Rempelos, L.; Troyanos, Y.; Leifert, C.; Markellou, E. *Reynoutria sachalinensis* extract elicits salicylic acid-dependent defense responses against powdery mildew. *Sci. Rep.* **2020**, *10*, 3517. [CrossRef] [PubMed]
21. Adaskaveg, J.E.; Michailides, T.; Eskalen, A. *Fungicides, Bactericides, Biocontrols, and Natural Products for Deciduous Tree Fruit and Nut, Citrus, Strawberry, and Vine Crops in California 2025*; University of California Integrated Pest Management Program: Davis, CA, USA, 2025. Available online: https://ipm.ucanr.edu/legacy_assets/PDF/PMG/fungicideefficacytiming.pdf (accessed on 2 March 2026).
22. Compant, S.; Samad, A.; Faist, H.; Sessitsch, A. A review on the plant microbiome: Ecology, functions, and emerging trends in microbial application. *J. Adv. Res.* **2019**, *19*, 29–37. [CrossRef] [PubMed]
23. Chen, X.H.; Koumoutsi, A.; Scholz, R.; Borriss, R. More than anticipated production of antibiotics and other secondary metabolites by *Bacillus amyloliquefaciens* FZB42. *J. Mol. Microbiol. Biotechnol.* **2010**, *18*, 61–74. [CrossRef] [PubMed]
24. Raaijmakers, J.M.; de Bruijn, I.; Nybroe, O.; Ongena, M. Natural functions of lipopeptides from *Bacillus* and *Pseudomonas*: More than surfactants and antibiotics. *FEMS Microbiol. Rev.* **2010**, *34*, 1037–1062. [CrossRef] [PubMed]
25. Hall, M.E.; Cadle-Davidson, L.; Fang, Z.; Wilcox, W.F. A new method for extracting DNA from the grape berry surface, beginning in the vineyard. *Heliyon* **2019**, *5*, e02597. [CrossRef] [PubMed]
26. Boulet, J.-C.; Meudec, E.; Ducasse, M.-A.; Abi-Habib, E.; Le Gall, S.; Falourd, X.; Bakan, B.; Traore, A.; Lucchi, G.; Gourrat, K.; et al. Insights into multiscale chemical characterisation for the understanding of berry maturation. *OENO One* **2025**, *59*, 8286. [CrossRef]
27. Chelius, M.K.; Triplett, E.W. The diversity of Archaea and Bacteria in association with the roots of *Zea mays* L. *Microb. Ecol.* **2001**, *41*, 252–263. [CrossRef] [PubMed]
28. Gardes, M.; Bruns, T.D. ITS primers with enhanced specificity for basidiomycetes—Application to the identification of mycorrhizae and rusts. *Mol. Ecol.* **1993**, *2*, 113–118. [CrossRef] [PubMed]
29. White, T.J.; Bruns, T.; Lee, S.; Gelfand, D.H.; Sninsky, J.J. Amplification and direct sequencing of fungal ribosomal RNA genes for phylogenetics. In *PCR Protocols: A Guide to Methods and Applications*; Innis, M.A., Gelfand, D.H., Sninsky, J.J., White, T.J., Eds.; Academic Press: New York, NY, USA, 1990; pp. 315–322. [CrossRef]
30. Deng, S.; de Hoog, S.D. Towards stable nomenclature for clinically relevant fungi. *iFungi* **2026**, *1*, 9670010. [CrossRef]

31. Yue, J.C.; Clayton, M.K. A similarity measure based on species proportions. *Commun. Stat. Theory Methods* **2005**, *34*, 2123–2131. [CrossRef]
32. Robertson, C.E.; Harris, J.K.; Wagner, B.D.; Granger, D.; Browne, K.; Tatem, B.; Feazel, L.M.; Frank, D.N. Explicet: Graphical user interface software for metadata-driven management, analysis, and visualization of microbiome data. *Bioinformatics* **2013**, *29*, 3100–3101. [CrossRef] [PubMed]
33. Hammer, Ø.; Harper, D.A.T.; Ryan, P.D. PAST: Paleontological Statistics Software Package for Education and Data Analysis. *Palaeontol. Electron.* **2001**, *4*, 1–9. Available online: https://palaeo-electronica.org/2001_1/past/issue1_01.htm (accessed on 2 March 2026).
34. R Core Team. *R: A Language and Environment for Statistical Computing*; R Foundation for Statistical Computing: Vienna, Austria, 2021. Available online: https://www.R-project.org/ (accessed on 2 December 2025).
35. Oksanen, J.; Simpson, G.L.; Blanchet, F.G.; Kindt, R.; Legendre, P.; Minchin, P.R.; O'Hara, R.B.; Solymos, P.; Stevens, M.H.H.; Szoecs, E.; et al. *Vegan: Community Ecology Package*, R Package Version 2.6-10; 2025. Available online: https://CRAN.R-project.org/package=vegan (accessed on 12 October 2026).
36. Teixeira, A.; Martins, V.; Gerós, H. From the vineyard soil to the grape berry surface: Unravelling the dynamics of the microbial terroir. *Agric. Ecosyst. Environ.* **2024**, *374*, 109145. [CrossRef]
37. Zhang, J.; Wang, E.T.; Singh, R.P.; Guo, C.; Shang, Y.; Chen, J.; Liu, C. Grape berry surface bacterial microbiome: Impact from the varieties and clones in the same vineyard from central China. *J. Appl. Microbiol.* **2019**, *126*, 204–214. [CrossRef] [PubMed]
38. Bulgari, D.; Casati, P.; Brusetti, L.; Quaglino, F.; Brasca, M.; Daffonchio, D.; Bianco, P.A. Endophytic bacterial diversity in grapevine (*Vitis vinifera* L.) leaves described by 16S rRNA gene sequence analysis and length heterogeneity-PCR. *J. Microbiol.* **2009**, *47*, 393–401. [CrossRef] [PubMed]
39. Compant, S.; Clément, C.; Sessitsch, A. Plant growth-promoting bacteria in the rhizo- and endosphere of plants: Their role, colonization, mechanisms involved and prospects for utilization. *Soil Biol. Biochem.* **2010**, *42*, 669–678. [CrossRef]
40. West, E.R.; Cother, E.J.; Steel, C.C.; Ash, G.J. The characterization and diversity of bacterial endophytes of grapevine. *Can. J. Microbiol.* **2010**, *56*, 209–216. [CrossRef] [PubMed]
41. Knief, C. Analysis of plant–microbe interactions in the era of next-generation sequencing technologies. *Front. Plant Sci.* **2014**, *5*, 216. [CrossRef] [PubMed]
42. Kutschera, U. Plant-associated Methylobacteria as co-evolved phytosymbionts: A hypothesis. *Plant Signal. Behav.* **2007**, *2*, 74–78. [CrossRef] [PubMed]
43. Martins, G.; Lauga, B.; Miot-Sertier, C.; Mercier, A.; Lonvaud, A.; Soulas, M.-L.; Soulas, G.; Masneuf-Pomarède, I. Characterization of epiphytic bacterial communities from grapes, leaves, bark and soil of grapevine plants grown under different conditions and their relationships. *PLoS ONE* **2013**, *8*, e73013. [CrossRef] [PubMed]
44. Wei, Y.-J.; Wu, Y.; Yan, Y.-Z.; Zou, W.; Xue, J.; Ma, W.-R.; Wang, W.; Tian, G.; Wang, L.-Y. High-throughput sequencing of microbial community diversity in soil, grapes, leaves, grape juice and wine of grapevine from China. *PLoS ONE* **2018**, *13*, e0193097. [CrossRef] [PubMed]
45. Iorizzo, M.; Bagnoli, D.; Vergalito, F.; Testa, B.; Tremonte, P.; Succi, M.; Pannella, G.; Letizia, F.; Albanese, G.; Lombardi, S.J.; et al. Diversity of fungal communities on Cabernet and Aglianico grapes from vineyards located in Southern Italy. *Front. Microbiol.* **2024**, *15*, 1399968. [CrossRef] [PubMed]
46. Bekris, F.; Papadopoulou, E.; Vasileiadis, S.; Karapetsas, N.; Theocharis, S.; Alexandridis, T.K.; Koundouras, S.; Karpouzas, D.G. Vintage and terroir are the strongest determinants of grapevine carposphere microbiome in the viticultural zone of Drama, Greece. *FEMS Microbiol. Ecol.* **2025**, *101*, fiaf008. [CrossRef] [PubMed]
47. Nardi, T.; Gaiotti, F.; Tomasi, D. Characterization of indigenous microbial communities in vineyards employing different agronomic practices: The importance of trunk bark as a source of microbial biodiversity. *Agronomy* **2021**, *11*, 1752. [CrossRef]
48. Lorenzini, M.; Zapparoli, G. Characterization and pathogenicity of *Alternaria* spp. strains associated with grape bunch rot during post-harvest withering. *Int. J. Food Microbiol.* **2014**, *186*, 1–5. [CrossRef] [PubMed]

Disclaimer/Publisher's Note: The statements, opinions and data contained in all publications are solely those of the individual author(s) and contributor(s) and not of MDPI and/or the editor(s). MDPI and/or the editor(s) disclaim responsibility for any injury to people or property resulting from any ideas, methods, instructions or products referred to in the content.